

**Novel polysaccharide hybrid scaffold loaded with hydroxyapatite:
Fabrication, bioactivity, and *in vivo* study**

Khairy M. Tohamy¹, Islam E. Soliman¹, Mostafa Mabrouk^{2,5}, Shaimaa ElShebiney³,
Hanan H. Beherei², Mohamed A. Aboelnasr¹ and Diganta B. Das^{4,5}

¹Biophysics Branch, Faculty of Science, Al-Azhar University, Nasr City 11884,
Cairo, Egypt.

²Refractories, Ceramics and Building materials Department, (Biomaterials
group), National Research Centre, 33El Bohouth st.(former EL Tahrirst.)-
Dokki- Giza- Egypt P.O.12622.

³Department of Narcotics, Ergogenic Aids and Poisons, Medical Research
Division, National Research Centre, Giza, Egypt, Affiliation ID: 60014618.

⁴Department of Chemical Engineering, Loughborough University,
Loughborough LE113TU, Leicestershire, UK.

**Submitted for consideration, review and publication in
Journal of Materials science and engineering C**

January 2018

_____ ⁵To whom correspondence should be addressed (e-mail:
mostafamabrouk.nrc@gmail.com and D.B.Das@lboro.ac.uk)

Abstract

The main goal of this study was to produce a novel porous scaffold for rapid *in vivo* bone healing behavior. Lyophilization technique was used to produce this highly porous hybrid scaffold from Na-alginate (S) and hydroxyethylcellulose (HEC) impregnated with different concentration of hydroxyapatite (HA). After cross-linking the scaffolds, their incubation was carried out in simulated body fluid (SBF) for 4 weeks at 37°C to investigate their bioactivity. A number of techniques were employed (e.g., XRD, FTIR, SEM, EDX, and texture analyzer) to characterize the designed scaffolds. It was observed that the mechanical properties of the scaffolds increase deformation energy ($182\pm 16 \text{ J/m}^3$) and rigidity gradient ($19.44\pm 0.85 \text{ Pa}$) after loading with HA. Furthermore, the scaffolds were implanted in femur critical size defects (2mm) of adult male Wistar rats for 6 weeks. *In vitro* and *in vivo* analyses demonstrated impressive bioactivity and biocompatibility for the prepared scaffolds, especially those containing HA. Based on the obtained results we conclude that the designed scaffolds are promising solutions for bone regeneration applications.

Keywords: Porous hybrid scaffolds; Polysaccharides; Biocompatibility; Mechanical properties; Rapid bone regeneration.

1-Introduction

Tissue engineering (TE) is an interdisciplinary field that applies key principles from chemistry, biology and materials science to comprehend the structural relationships (i.e., dependence of material characteristic on other factors) and the expansion of biological replacement that reestablish, keep up or enhance the tissues functions [1, 2]. TE depends on three essential parameters, namely, matrix (3D scaffolds), cells and growth factors. Scaffolds are fabricated to work temporarily as artificial extracellular matrix (ECM) whilst keeping in mind

the end goal of helping cell propagation and infiltration through three-dimensional (3D) tissue development [3, 4]. Therefore, a typical scaffold should mimic the normal ECM in human body, which supports cells growth on the material from surrounding tissues [5-7]. The scaffolds should provide suitable mechanical properties to the bone defect site in order to maintain the physiological function of the defected site. In addition, the surface topography and porosity are important scaffold characteristics for cells attachment, propagation and proliferation [8, 9]. Natural and synthetic biopolymers [10-12] have been utilized as scaffolds for TE applications since they have good biocompatibility and biodegradability. In order to fully understand the context of this work we now discuss a few relevant points below.

To prepare the scaffolds in this work, we have utilized freeze-drying which has been shown to produce highly porous scaffolds and interconnected pores which closely resemble the topography features of ECM. In the previous studies it has been used to prepare nano- and micro-porous scaffolds from polymer solutions in a wide range of pore diameters [13]. The scaffolds prepared by freeze-drier also have unique properties such as high surface area-to-volume ratio, high porosity and range of pore diameters. It is worth highlighting that the features of the scaffold should be well suited to perform all the aforementioned functions and to suit vast number of cells to growth within the scaffolds. Open connected pore system improves the dispersion rate of supplements and waste products[14]. The material should be biocompatible with appropriate mechanical behavior to withstand cell culture conditions. Also, attachment of cells to the biomaterial surface is very important factor.

As the chosen polymer, alginate is used in this work. It is a randomly anionic linear polysaccharide polymer derived from brown sea algae and some types of bacteria. It is composed of diverse ratios of two types, namely, β -L guluronic acid (G) and α -D mannuronic acid (M) units [15-18]. It is dissolvable in some solution such as water at ambient temperature and form stable gels in the presence of divalent cations, like Ca^{2+} , Ba^{2+} , Sr^{2+} [19, 20]. Since it is a hydrophilic polymer, the alginate scaffolds swell easily and allows sufficient penetration of cells inside the matrix scaffold. Alginate breakdowns into simple glucose type,

which is totally absorbable [14]. There are some of remarkable achievements of alginate scaffolds and collective characterized (relatively low cost, hydrophilicity and biocompatible natural polymer) [21], which make it an important biopolymer in pharmaceutical field such as cell encapsulation, dental impression materials and wound dressings.

HEC is a non-ionic polysaccharide polymer with β (1 \rightarrow 4) glycosidic linkage held together with H-bonds. It is inexpensive and broadly utilized as a part of different pharmaceutical structures, wound dressing and wound remodeling system [22, 23]. Previous studies have combined alginate and HEC in order to maximize their usage in different fields. For example Swayampakula et al [24] synthesized membrane by blending sodium alginate (SA) with hydroxyethylcellulose (HEC) and utilized phosphoric acid as ionic cross-linker. Choonara et al [25] prepared gelspheres from alginate-hydroxyethylcellulose (Alg-HEC) with different cross-linker salt such as Ca^{2+} , Zn^{2+} and Ba^{2+} chloride for the controlled release. Russo et al [26] prepared thin films by blending the aforementioned polysaccharides and/or polyglycerol to improve thermal and mechanical parameters and water absorbability.

However, polymeric scaffolds possess some limitations in the treatment of bone defect due to their poor bioactivity. To overcome these limitations incorporation of inorganic filler within the polymeric scaffold matrix is a realistic solution. Among various inorganic biomaterials, hydroxyapatite (HA) has gained a wide interest in the development of organic/inorganic composite scaffolds for tissue engineering applications due to their impressive biocompatibility, strong resorbability, good cell adhesiveness, and outstanding bioactivity [27-29]. Accordingly, the main objective of this work was the synthesis and characterization of a new porous hybrid of two polysaccharides loaded with HA. Furthermore, both in vitro and in vivo bioactivity studies were conducted and the prepared scaffolds were fully characterized.

2. Experimental

2.1 Materials

All materials utilized in this research are commercially attainable, sodium alginate (S) with molecular weight (MW) of 500,000 g/mol, hydroxyethylcellulose(HEC), MW= 90,000g/mol, calcium chloride, MW=147.02

g/mol and the reagents of SBF were obtained from Sigma Aldrich, Germany. Moreover, the HA reagents, calcite (Anala R, specified minimum assay 99.0 % CaCO₃, 14µm mean particle size, BDH Laboratories Ltd.) and DCPA (Phosphor Grade, particle size 30-50 µm, Lumifax Ltd.).

2.2. Preparation of hydroxyapatite filler

Solid state technique was employed to fabricate hydroxyapatite (HA) powder as previously mentioned by Morgan et al [30] with small modifications. The following chemical substances, namely, CaCO₃ and CaHPO₄, were used as raw materials. 81.666g of CaHPO₄ and 39.930g of CaCO₃ were milled by using a ball milling machine for 1h to form a homogenous mixture. Monoclinic hydroxyapatite was obtained by firing the mixture at 1000°C under atmospheric conditions for 3h. The HA was formed according to the following reaction:



2.3. Synthesis of S/HEC/HA composite porous scaffolds

Freeze dryer technique was employed to prepare the S/HEC/HA scaffolds. Firstly, S and HEC (20%^{w/v}) solution was prepared by dissolving S and HEC powders in distilled water and were stirred kept for 1h at 60°C. HA powder was mixed with the polymers hybrid according to Table 1. The resulting mixtures were casted in Petri dishes and kept at -18°C for overnight, and then, the samples were lyophilized for 24h at -56°C. Finally, the scaffolds were immersed in 5% CaCl₂ solution up to 3h for crosslinking. Moreover, the crosslinked scaffolds were washed three times by distilled water, dried at room temperature and kept in the desecrator for further analysis.

INSERT TABLE 1

2.4 Characterization of fabricated scaffolds

The thermal manners of the hybrid composite and native polymer were determined by differential scanning calorimetry (DSC) and thermal gravimetric analysis (TGA) using a computerized SETARAM labsys™ TG-DSC thermal analysis system range of 25–1000°C with a heating rate of 10°C/min. In DSC

analysis, a small part of all scaffolds (10 mg) was placed into a platinum crucible, heated from room temperature to 1000°C with heating rate 10°C/min under a constant flowing atmosphere. XRD paradigm of the specimens was examined by utilizing [Axs D8 ADVANCE], [$Cu\alpha = 1.54056\text{\AA}$] radiation. XRD was taken at 2θ angle range of 10–70 and the operation conditions were: scan move size 0.02 (2θ) and scan move time 0.05 s. XRD is a useful method to confirm the amorphous or crystalline nature of the samples. The tested samples were crashed in an agate mortar before measuring. Fourier transform infrared (FTIR) spectroscopy measurements were recorded at room temperature in the range 400–4000 cm^{-1} to evaluate the effect of HEC and HA on the chemical integrity of the composite scaffolds, with Model 580, Perkin-Elmer. Dried composite scaffolds were ground and mixed thoroughly with potassium bromide at a ratio of 1:5 (Sample: KBr).

The microstructural properties of the scaffold samples before and after immersion in SBF were determined by Scanning Electron Microscope (SEM) (demonstrate XL30, Philips) connected with component investigation of an X-ray detector (EDX) unit, with 20-25 kV quickening voltage, amplification image up to 400,000X and its determination is done at a scale of 3.5 nm. SEM micrographs were acquired subsequent to covering the samples with gold for excellent observation, utilizing Edwards 5150 sputter covering (England). The Brunauer Emmett-Teller (BET) calculations for surface area [31] and BJH calculations for pore size [29] distribution for the desorption branch of the isotherm of the samples were determined by nitrogen adsorption at -196°C using a Micromeritics ASAP2020 surface area and porosity analyzer (USA). Briefly, the samples (100mg) of the lyophilized composite scaffolds were underwent two stages of analysis, first following a degassing stage at 200°C for 3h and thereafter an nitrogen absorption and desorption cumulative phase for accurate analysis of surface area.

The mechanical properties of the composites scaffolds were evaluated by measuring the Rigidity Gradient (RG) and Deformation Energy (DE) of prepared sample using a Texture Analyzer (TA.XTplus Stable Micro systems, Surrey, UK). The DE is defined as the absorbed energy that causes deformation of the elastic

scaffold; The RG refers specifically to the scaffold unit migration guided by gradients in substrate rigidity. Both DE and RG were used as two system examination to estimate mechanical behavior for prepared composite sample. The specimens were evenly cut from the most homogeneous region of the scaffolds to form blocks with dimensions of $10 \times 5 \times 5 \text{ mm}^3$. These sample scaffolds were situated between parallel plates utilizing a component EMIC DL 3000 and compressed with a crosshead speed of 0.5 mm/min and a 1.0 kN load cell. Minimum three pieces ($n=3$) of each composite scaffold specimens were investigated[32-34].

2.5 *In vitro* studies

2.5.1. *In vitro* Bioactivity in SBF

Simulated body fluid (SBF) was used to determine the bioactivity of the scaffolds samples, the scaffolds immersed in SBF at 37°C as earlier reported[34]. The scaffolds were submerged ($10 \times 10 \times 5 \text{ mm}^3$) in SBF (60 ml, $\text{pH}=7.4$) and preserved in a dynamic water bath at 37°C up to 28 days [35-37]. At the end of each immersion period, the specimens were filtered, washed three times by distilled water, and air dried at room temperature. The changes happened on the scaffolds surface were then examined through XRD, SEM, EDX and FTIR estimations as described in [38].

2.6 *In vivo* experiments

The *in vivo* biocompatibility and osteointegration of the prepared scaffolds were evaluated against a rat critical size fumer as described in [39]. Prior to implantation in the rats, equal specimen of each scaffold sample was cut and soaked in deionized water for 10min in order to soften the samples. Six rats were used for each scaffold to determine the statistical significances. Adult male Wistar rats ($185 \pm 20\text{g}$) were obtained from the breeding colony of VACSERA, Helwan, Egypt. The animals were kept for 7 days for acclimatization in standard conditions. Chow diet and water were provided ad libitum. Research protocol was approved by the Animal Care Committee (registration number # 16261) of the National Research Centre, Egypt, which follows the guidelines of the National

Institutes of Health Guide for Care and Use of Laboratory Animals. Rats were anaesthetized using chloral hydrate (400mg/kg, i.p.) in temperature controlled chamber.

A lateral incision was made and femur was exposed, 2mm drill hole was made at the diaphyseal part of the femur for control group without filling holes. On the other hand, other 5th group (S, SH, SH10, SH20 and SH40) the bone debris was removed and the hole was filled with the prepared scaffolds. Incision was sutured with surgical nylon filament and cleansed with betadine. A bandage was made along the hind limb and kept for 7 days. Rats were caged after the surgery individually to minimize trauma. Post-operative management was achieved by administration of cefotaxime (100mg/kg, i.p., every 12h) and ketolac (1.5mg/kg, i.p., twice daily). X-ray was performed at the 7th day to ensure right placement of the limb. Twelve weeks after the surgery, the animals were sacrificed. Femurs and liver were dissected, cleaned in saline, eye-examined and kept in 10% formol-saline for further examination. Sera were collected at one month point and stored in -80°C till analysis.

2.6. 1 Histological examination

Bone samples of rats in different groups were fixed and decalcified in formic acid. Liver samples were fixed in 10% formol-saline solution. Washing was done in tap water, and then serial dilutions of alcohol (methyl, ethyl and absolute ethyl) were used for dehydration. All specimens were cleared in xylene and embedded in paraffin at 56°C in a hot air oven for 24h. Paraffin bees wax tissue blocks were prepared for sectioning at 4 microns thickness by slide microtome. The obtained tissue sections were collected on glass slides, deparaffinized, and stained by hematoxylin and eosin stain for examination through the light electric microscope [37].

2.6.2 Blood biochemistry analysis

Serum liver enzymes; GPT and GOT were measured by commercial kits purchased from Biovision, Egypt. Measurements were done spectrophotometrically. The serum level of reduced glutathione (GSH) was also

determined spectrophotometrically according to the method described by Beutler et al. [38] using Ellman's reagent and the color produced was detected at $\lambda=412\text{nm}$. Lipid peroxidation products collectively measured as malondialdehyde (MDA) were colorimetrically assayed as described by Uchiyama and Mihara[39].

Statistical analysis

All data in the study is represented as mean \pm standard error of mean. Statistical significance was tested by one-way ANOVA followed by Tukey's post-Hoc test of comparison at 95% confidence level.

3. Results

3.1 TGA analysis

The thermo-gravimetric data are reported in Fig.1 and Table 2, where S and HEC are both different in terms of absorbed water and thermal decomposition. In the TGA curves we can clearly distinguish four regions. The first region is from the room temperature to 180°C , where the mass loss was associated with the elimination of water; the second region is between 180°C and 350°C , where the mass loss was attributed to the degradation of polysaccharides network; third region is above 350°C to $\approx 550^{\circ}\text{C}$, and it may corresponds to degradation of calcium alginate, degradation step, Na_2CO_3 and other carbonaceous materials. The final region above 550°C is associated with the degradation $\text{Ca}(\text{OH})_2$ and crystallization temperature.

INSERT FIGURE 1

INSERT TABLE 2

3.2 Mechanical properties

Deformation energy (DE) and the rigidity gradient (RG) were evaluated for the S/HEC/HA scaffolds in dry conditions. It was observed that DE results refer to decrease from S to SH (100.00 ± 10.00 to 90.00 ± 10.50 Joule/ m^3), after that gradually increase with filler content increase 145.00 ± 13.00 , 163.00 ± 14.00 and 182.00 ± 16.00 Joule/ m^3 for SH10, SH20 and SH40, respectively (Fig 2 a). Also, RG values were decreased for SH

(5.80 ± 0.52 Pa) compared to S (6.90 ± 0.39 Pa), after that they gradually increase with filler content increase 11.70 ± 0.63 , 16.70 ± 0.74 and 19.44 ± 0.85 Pa for SH10, SH20 and SH40, respectively (Fig 2 b). The results indicated that the higher HA concentration the higher DE and RG are obtained compared with the S and HEC native polymers. These results could be explained due to the reinforcing effect of HA filler.

INSERT FIGURE 2

3.3 Surface Area and Porosity

The BET surface area, pore volume and average pore diameter measurements of pure sodium alginate (S), the hybrid of the two native polymers (S/HEC) with two selected concentration of HA are demonstrated in Fig. 3 and Table 3. It was observed that the hybrid increased the surface area and the total pore volume. Furthermore, presence of HA in the composites decreased the surface area compared to S/HEC hybrid. These results could be explained due to that some pores of the native polymers scaffolds was blocked by the presence of HA, thus, the hybrid scaffold with different concentration of HA retain a decrease surface area and a appropriate pores volume.

INSERT FIGURE 3

3.4 XRD before and after soaking in SBF

Fig. 4a shows the XRD patterns of the composite synthesized by freeze-drying method before immersed in SBF. It is worthwhile to note that, the diffraction peaks of S and SH samples exhibited completely amorphous nature with a broad peak between 20 and 40° (2θ), which is attributed to the polymer network [40]. HA loaded within the native polysaccharides hybrid (SH40) exhibited dominant peaks of XRD pattern in Fig. (4a) that was referred to HA matched with standard card of JCPDS 76-0694.

INSERT FIGURE 4

Fig. 4b showed the XRD patterns of the prepared scaffolds after immersed for prolonged time 28 days in SBF. In general, there were four sharp peaks located at 2θ , 25.6° , 31.76° , 32.16° and 33° was showed after immersion period, these diffraction peaks were allocated to (1 1 1), (0 0 2), (2 1 1), (3 0 0) planes and showed the arrangement of HA layer over the sample scaffolds surface as per the standard JCPDS document no. (82-1943), the broad diffraction peak at (2θ) running from 31.2° : 34.3° relates to interference of (2 1 1), (1 1 2), (3 0 0) and (2 0 2) refers to good crystallization hydroxyapatite phase [41-43]. The intensity of apatite peaks increased with the increasing of HA concentrations. This increment was attributed to the increased precipitation of Ca^{2+} and PO_4^{3-} ions on the scaffolds surfaces [44].

3.5.FTIR analysis

FTIR spectra of S and SH are represented in Fig. 5a. The spectrum of S shows the characteristic peaks in the range $1595\text{--}1610\text{cm}^{-1}$ and in the range $1405\text{--}1415\text{cm}^{-1}$ due to the COO^- asymmetric and symmetric stretching bands. In the fingerprint region of alginate, several absorption bands used to estimate the ratio mannuronic/guluronic like bands located at 817 and 877cm^{-1} assigned to C-C-H, skeletal C-C, C-O-H and C-O-C symmetric vibration of 1,4-glycosidic link [45], 1036cm^{-1} (C-O-C stretching). In the SH spectrum no noticeable features with respect to the spectrum of S were observed. Both spectra showed characteristic bands in the range $3200\text{--}3550\text{cm}^{-1}$ corresponding to O-H stretching vibrations. However, the characteristic (O-H deformation) band in both S and SH in rang $610\text{--}620\text{cm}^{-1}$, showed a slight shift to lower wavenumber (from 619 in S to 611cm^{-1} in SH. This shift may be related to the bonding between S and HEC groups. The intensity of this band was increased through Ca cross-linking [40], suggesting a good distribution of HEC particles within the alginate matrix. In addition, the presence of HA in the prepared composite scaffolds was also confirmed by FTIR spectra. In details, the absorption bands corresponding to the symmetric and asymmetric stretching modes of phosphate groups of HA located at 1029 , 1092 , 961 , 605 and 560cm^{-1} , respectively, were observed.

Moreover, the FTIR spectra of the prepared scaffolds after immersed in SBF for 28 days are demonstrated in Fig 5b, Generally, two bands at 564cm^{-1} and 603cm^{-1} were observed for all the prepared scaffolds after immersion in SBF [46] as well as broad bands observed at 1024cm^{-1} and 1108cm^{-1} confirming the presence of calcium phosphate precipitates [47, 48]. The precipitation of calcium phosphate was found to be dependent on the HA concentration in the scaffolds as confirmed by the characteristic O-H bands located at 1637 and 3419cm^{-1} , that increased gradually from S and SH to SH40. This result could be explained due to the hydrogen bonds and electrostatic forces presented among ions and groups in the composite scaffolds. Particularly, chemical interaction between -C=O groups in S biopolymer and charged groups such as Ca^{2+} and PO_4^{3-} of the HA filler. Additionally the coordination bonds that were initiated between Ca^{2+} groups of HA as filler and -COO^- group of S as a network polymer were early reported [49, 50]. Thus, the high concentrations and uniform distribution of HA particles in the S/HEC hybrids enhanced the bioactivity of the scaffolds. Furthermore, it is well-known that the higher content of HA in the composite, the better bioactivity could be attained [51, 52]

INSERT FIGURE 5

3.6. SEM Analysis

From Fig. 6 shows the S/HEC biopolymer scaffolds microarchitecture with and without HA. Generally, all the fabricated scaffolds were consists of a highly porous structure with lamellae orientation. Moreover, rougher pore walls were observed for scaffold SH40 (Fig. 6b) compared to scaffold SH (Fig. 6a). This phenomena could be attributed to the presence of HA particles within the hybrid matrix. Furthermore, growth of white granular layers were observed on the scaffold surfaces after 28 days of scaffolds immersion in SBF.

The EDX analysis of these layers confirmed to be calcium phosphate layers with different Ca/P depending on the presence of HA as shown in Fig 6 (e3 and f3). In details, both EDX spectra confirmed the presence of multi peaks, for the following elements P, O, Cl, Ca, k, and Na. A clear enhancement of the Ca and P peaks together with Ca/P molar ratio of 1.71. This observation suggests that a good bonding exist between the two

organic and inorganic components, which are known to be a requisite necessary to assure a good integrity and functionality of the bone cell.

In addition, the difference in the intensity of calcium phosphate precipitations on the scaffolds surfaces was investigated by treatment with the flooding algorithm in SXWM software (Fig 6 (e1,2 and f1,2)). Notable contrast difference in the surface morphology between the two investigated scaffolds after soaking in SBF was obvious, demonstrating the arrangement of calcium phosphate layers with different amount on the scaffolds surface.

INSERT FIGURE 6

3.7 *In vivo* results

3.7.1 Histological analysis

Based on the promising results obtained *in vitro* in terms of biomineralization, and calcium phosphate formation on scaffolds surface, an *in vivo* study was performed to evaluate the potentiality of the fabricated scaffolds in the treatment of bone defects and to improve the osteointegration of scaffolds implants. The control rats with a burr hole without any matrix fillers showed focal osteonecrotic area at the margins of the burr hole without remarks for the osteoblast proliferation (Fig. 7a). Filling the whole with pure sodium alginate (S) scaffold initiated the healing process at that time point and osteoclasts and osteoblasts cells were observed at the peripheral zone (Fig. 7b). In details, almost filled by more mature trabecular bone that contained osteocytes and many reversal lines that begin to enclose more or less large marrow cavities. Small areas of calcified cartilage were evident within the lamellar bone. On the top of the lamellar bone still there was a transitional zone of osteoid tissue filled with many osteocytes. Finally on the top we could see zone of endochondral ossification intermingled with areas of calcified cartilage. Examining the femur after filling the burr hole with two native polymers S/HEC (SH) without addition of HA showed granulation tissue with inflammatory cell infiltration and fibrotic cluster at the hole.

This inflammation starts to subside after HA addition (Fig.7c) (scaffolds SH10) and the hole was filled with granulation tissue. Particularly, the defect was fully filled with

dense fibrous connective tissue that was invaded by many chronic inflammatory cells. On the edges of the connective tissues mature bone trabeculae was noted. Fig.7(d) showed that the defect is filled with cellular and fine fibrous connective tissue with few chronic inflammatory cells. A continuous layer of lamellar bone observed having few numbers of osteocytes and reversal lines indicating remodeling. In group 5 (scaffolds SH20) massive osteoblast formation was noticed in the hollow area of femur (Fig.7e), the base of the defect filled with long and thin interconnected bone lamellae that appeared immature with increased number of osteocytes. The newly formed bone lamellae enclosing more or less large marrow cavities .on the top of lamellar bone osteoied tissue was observed. Areas of granulation tissue still evident and large area occupied with fibrous connective tissue beneath the granulation tissue. Group 6 (SH40) there was a focal area of calcification remodeling bone which confirmed the scaffold resorption and formation of new bone tissue (Fig.7f). Specifically, the defect filled with dense fibrous connective tissue that showed separate areas of calcified cartilages. Some parts of the calcified cartilage begin to be replaced by bone in form of calcified bone matrix.

In order to assess the effect of implanted scaffolds on the vital organs of the under investigated rats, liver histological studies were conducted as shown in Fig. 8. According to the results of histological sections of liver, no histopathological alterations among different groups compared to control rats. Photomicrographs showed normal hepatocytes and micro vessels with normal central vein and surroundings. The centrilobular vein is clear, and the cells inside section liver are arranged in radial lines. From the obtained results, all the scaffold implants do not have side effects on the liver function after 6 weeks of implantation and do not cause even necrotic lesions.

INSERT FIGURE 7

INSERT FIGURE 8

3.7.2 Blood biochemical analysis

Aspartate amino-transferase (AST) or serum glutamic-oxalo acetic transaminase (SGOT), and alanine amino-transferase (ALT) or serum glutamic-pyruvic transaminase (SGPT), which is an enzyme produce in liver for the amino acid metabolism. In addition, ALT enzymes used to break down and transfers food into energy, Glutathione (GSH) is often referred to as the body's master antioxidant, also an essential component to the

body's natural defense system. Serum MDA levels is still the most commonly applied assay for lipid peroxidation in biomedical sciences. Since MDA is one of the major aldehydes formed after breakdown of lipid hydroperoxides, therefore, it is considered a good biomarker of the involvement of free radical damage in pathologies associated to oxidative stress. In this study serum GPT, GOT, GSH, and MDA biomarkers showed no significant variation for all the scaffolds samples after implantation time periods. The biomarkers were comparable to normal control levels in all groups when compared statistically normal results see Fig 9, therefore, the incorporation of HA in the hybrid biopolymers scaffold or even two native polymers hybrid have not affect or causes any hepatotoxicity markers in liver rats.

INSERT FIGURE 9

4. Discussion

Bone can be considered as a nano-composite material made up of collagen, protein fibres threading through HA mineral phase, which makes up about 60–70wt% of the bone structure. Based on a biomimetic mechanism, S/HEC/HA composite scaffold was prepared in order to produce a similar composition to that of natural bone. The organic S/HEC hybrid network loaded with HA granules, similar to the interactions that exist between the components of normal bone [49, 50, 54]. Electrostatic forces and hydrogen bonds exist among the ions and groups in the composite material, such as interactions between Ca^{2+} and PO_4^{3-} charged groups of HA and $-\text{C}=\text{O}$ in S, as well as the coordination bonds that are formed between the $-\text{COO}^-$ group of S and OH^- in both S, HEC with Ca^{2+} group of HA as confirmed by FTIR results and the previous studies [49-57]. Therefore, the high proportion of HA and their uniform distribution in the hybrid matrix enable the scaffolding material to possess good biocompatibility, high bioactivity and suitable mechanical strength [55]. In addition, it is well-known that the higher HA concentration in the composite, the better bioactivity can be yielded by the implanted material [58, 59].

Microstructure results SEM Fig 6 and BET surface area of the prepared composite, revealed that, most of the pores were in the micro range from 89.5 ± 4.58 to $217.7\pm 10.87\mu\text{m}$ in diameter as shown in Fig3 and Table 3. It is worth to highlight that the pore diameters more than $50\mu\text{m}$ can easily facilitate the cell infiltration and bone mineralization [30].

Many efforts made in the design of scaffolds consisting of different polymers using both conventional and additive manufacturing techniques that have been recently reported [60,61]. Previous studies have demonstrated that S/HA composite material exhibited good mechanical properties similar to that of natural bone [22, 43]. Therefore, in this research work the proposed scaffolds formulations were fabricated aiming to achieve better porosity and mechanical properties. In details, the mechanical results of the S/HEC/HA scaffolds revealed that the composite scaffolds deformation energy increased with increasing of HA increasing and RG decreased with HA increasing. The obtained mechanical results were similar to the upper value of the strength of cancellous bone with suitable porosity required for cell infiltration and proliferation about 70% of scaffolds to create new bone tissue [51-54].

Osteoblasts are anchorage-dependent cells and their attachment to scaffolds depends on the surface area and the porosity of the scaffolds. The freeze-drying process produces scaffolds with small diameters and correspondingly high (surface area/volume ratios) that are suitable for osteoblast attachment from ECM, while permit for cell interpenetration and full migration. The interaction mechanisms that takes place between scaffolds and osteocytes are approximately understood. Relatively abundant proteins such as fibronectin, laminin, vitronectin, and collagen may first adsorb to the material surface [8]. Once such proteins adhere to the material's surface, cells are able to interact with the proteins through specific molecules on the surface of the cell. It is well-known that HA is deeply involved in the initial protein adsorption, such as vitronectin and fibronectin [19]. Consequently, proteins adsorbed from surrounding medium onto the scaffold, which then causes cells transportation. This is most favorable to the composite scaffolds and cause a good cell adhesion, after that cells proliferate on the scaffold surfaces. In the current study, HA has been shown to facilitated cell dispersion when blended into polysaccharide polymer scaffolds as early reported [12].

The formation of new bone on defect site occurred actually at the bony ends utilizing the scaffolds as a tissue reconstructing guide. This suggests that the positive effects on bone healing are truly due to the active role of the aECMs that have been applied as biofunctional addition of HEC and HA to native polymers. On the other hand it shows that the effects of blending with organic/organic hybrid seem to be mainly confined to the implant surface. For the complete critical size defects regeneration, must be on a 3D scaffolds that has the same surface morphology but promote in growth of new bone seem to be preferable with respect to potential clinical applications.

According to previous research, the *in vivo* decomposition of sodium alginate was described as unpredictable and uncontrollable clearance delay due to the fact lack of natural enzymes for alginate degradation in mammals [62]. Oxidation process is therefore often takes place prior to crosslinking [63], as used in this study, to allow for hydrolytic *in vivo* degradation of the implant. Furthermore, oxidized alginate molecules are easily eliminated by the kidneys [60], as were proved by the liver histology that there is no toxicity for all the groups [65,66] see Fig 8. Finally, pores are the favorable nucleation sites for cells attachment which must be found in scaffolds for bone regeneration usage. Pore properties like shape, size, volume and inorganic phase are importance key parameters that determine the usefulness of a scaffold. [64,65].

Conclusion

It can be concluded that the prepared scaffolds are promising in terms of their bioactivity and they could be used as materials for bone repair and tissue engineering. New scaffolds with highly porous structure were prepared from cheaply available polysaccharide polymers with HA filler by lyophilization technique. Addition of HEC had enhanced the microstructure of hybrid matrix compared to native alginate. Incorporation of HA within the hybrid matrix improved both mechanical behavior and bioactive deposition reaction. Furthermore, good interfacial bonding between the implanted composite scaffolds and extracellular fluid or physiological solution surrounding scaffolds, was governed by presence of porous structure which promoted the cells to penetrate inside the implanted scaffolds. This in turn, initiated the formation of new bone to repair the defected sites after short period (6 weeks). Moreover, the bio-safety of the fabricated scaffolds was confirmed by the normal blood results and liver histological analysis. All the

combined results support the implementation of the fabricated scaffolds in treatment of bone defects.

References

- [1].H. Zhang, H. Nie, S. Li, C.J.B. White, and L. Zhu, Crosslinking of electrospun polyacrylonitrile/ hydroxyethyl cellulose composite nanofibers, *Materials Letters*, 63 (2009) 1199-1202,.
- [2].K.T. Shalumon, N.S. Binulal, N. Selvamurugan, S.V. Nair, D. Menon, T. Furuike, et al., Electrospinning of carboxymethyl chitin/poly(vinyl alcohol) nanofibrous scaffolds for tissue engineering applications, *Carbohydrate Polymers*, 77(2009)863-869.
- [3].C.P. Barnes, S.A. Sell, E.D. Boland, D.G. Simpson, and G.L. Bowlin, Nanofiber technology: Designing the next generation of tissue engineering scaffolds, *Advanced Drug Delivery Reviews*, 59(2007) 1413-1433.
- [4].M.P. Prabhakaran, J. Venugopal, and S. Ramakrishna, Electrospun nanostructured scaffolds for bone tissue engineering, *Acta Biomaterialia*, 5 (2009) 2884-2893.
- [5].H.S. Yoo, T.G. Kim, and T.G. Park, Surface-functionalized electrospun nanofibers for tissue engineering and drug delivery, *Advanced Drug Delivery Reviews*, 61 (2009) 1033-1042.
- [6].Z.X. Meng, Y.S. Wang, C. Ma, W. Zheng, L. Li, and Y.F. Zheng, Electrospinning of PLGA/gelatin randomly-oriented and aligned nanofibers as potential scaffold in tissue engineering, *Materials Science and Engineering: C*, 30 (2010) 1204-1210.
- [7].J.M. Holzwarth. and P.X. Ma, Biomimetic nanofibrous scaffolds for bone tissue engineering, *Biomaterials*, 32 (2011) 9622-9629.
- [8].A.S. Asran, S. Henning, and G.H. Michler, Polyvinyl alcohol collagen hydroxyapatite biocomposite nanofibrous scaffold: Mimicking the key features of natural bone at the nanoscale level, *Polymer*, 51 (2010) 868-876.
- [9].M.C. Phipps, W.C. Clem, J.M. Grunda, G.A. Clines, and S.L. Bellis, Increasing the pore sizes of bone-mimetic electrospun scaffolds

comprised of polycaprolactone, collagen I and hydroxyapatite to enhance cell infiltration," *Biomaterials*, 33(2012) 524-534.

[10].Y.T. Jia, J. Gong, X.-H. Gu, H.-Y. Kim, J. Dong, and X.-Y. Shen, Fabrication and characterization of poly (vinyl alcohol)/chitosan blend nanofibers produced by electrospinning method, *Carbohydrate Polymers*, 67 (2007) 403-409.

[11].F. Yang, J.G.C. Wolke, and J.A. Jansen, Biomimetic calcium phosphate coating on electrospun poly (-caprolactone) scaffolds for bone tissue engineering, *Chemical Engineering Journal*, 137 (2008) 154-161.

[12].M.V. Jose, V. Thomas, K.T. Johnson, D.R. Dean, and E. Nyairo, Aligned PLGA/HA nanofibrous nanocomposite scaffolds for bone tissue engineering, *Acta Biomaterialia*, 5 (2009) 305-315.

[13]. J. Yan, Y. Miao, H. Tan, T. Zhou, Z. Ling, Y. Chen, X. Xing, X.Hu, Injectable alginate/hydroxyapatite gel scaffold combined with gelatin microspheres for drug delivery and bone tissue engineering. *Materials Science & Engineering C*, 63 (2016) 274-284.

[14].H. Suhaimi and D.B. Das (2016) Glucose diffusion in tissue engineering membranes and scaffolds: A review, *Reviews in Chemical Engineering*, 0(0), pp.0-0, ISSN: 0167-8299. DOI: 10.1515/revce-2015-0021.

[15].S. Gorgieva and V. Kokol, Synthesis and application of new temperature-responsive hydrogels based on carboxymethyl and hydroxyethyl cellulose derivatives for the functional finishing of cotton knitwear, *Carbohydrate Polymers*, 85 (2011) 664-673.

[16].H. Trieu and S. Qutubuddin, Poly (vinyl alcohol) hydrogels: 2. Effects of processing parameters on structure and properties, *Polymer*, 36 (1995) 2531-2539.

[17].J.A. Killion, L.M. Geever, D.M. Devine, J.E. Kennedy, and C.L. Higginbotham, Mechanical properties and thermal behaviour of PEGDMA hydrogels for potential bone regeneration application, *Journal of the Mechanical Behavior of Biomedical Materials*, 4 (2011) 1219-1227.

[18].I.W. Sutherland, Alginates. In *Biomaterials: Novel materials from Biological Sources*. (D. Bryon ed.), Stockton press, Newyork, 309 (1991).

- [19].J. Sun, and H. Tan, Alginate-Based Biomaterials for Regenerative Medicine Applications *Materials* 6 (2013) 1285–1309.
- [20].E.Y. Heo, N.R. Ko, M.S. Bae, et al., Novel 3D printed alginate–BFP1 hybrid scaffolds for enhanced bone regeneration. *Journal of Industrial and Engineering Chemistry*. 45(2017) 61-67.
- [21].K. Catherine and X. Peter, Ionically cross linked alginate hydrogels as scaffolds for tissue engineering. Part1.Structure, gelation rate and mechanical properties, *Biomaterials*, 22 (2001) 511-521.
- [22].F.H. Zulkifli, F. Shahitha, M.M. Yusuff, N.N. Hamidon and S. Chahal, Cross-Linking Effect On Electrospun Hydroxyethylcellulose/Poly(Vinyl Alcohol) Nanofibrous Scaffolds. *Procedia engineering* 53 (2013) 689-695.
- [23].M. Mabrouk, D.R. Chejaraa, J.A.S. Mulla, et al.,. Design of a novel crosslinked HEC-PAA porous hydrogel composite for dissolution rate and solubility enhancement of efavirenz, *International Journal of Pharmaceutics*,490 (2015), 429–437.
- [24].K. Swayampakula, S. Biduru, S. Sundergopal, K. Abburi, Blend membranes of sodium alginate and Hydroxyethylceloluse for pervaporation-based enrichment of t-butyl alcohol, *Carbohydrate Polymers*, 64 (2006) 425–432.
- [25].Y.E. Choonara, P. Viness, A.K. Riaz, N. Singh, C.D. Lisa, Mechanistic Evaluation of Alginate-HEC Gelisphere Compacts for Controlled Intrastratial Nicotine Release in Parkinson’s Disease. *J Pharm Sci*. 98(6) (2009) 2059-72.
- [26].R. Russo, M. Abbate, M. Malinconico, G. Santagata, Effect of polyglycerol and the crosslinking on the physical properties of a blend alginate-Hydroxyethylcellulose *Carbohydrate Polymers*, 82 (2010) 1061–1067.
- [27].S. Zhou, A. Bismarck, & J. Steinke, Interconnected macroporous glycidyl methacrylate-grafted dextran hydrogels synthesised from hydroxyapatite nanoparticl estabilised high internal phase emulsion templates. *J. Mater. Chem*. 22(2012) 18824-18829.

- [28]. R.M. Boehler, S. Shin, A.G. Fast, R.M. Gower, L.D. Shea, A PLG/HAp composite scaffold for lentivirus delivery. *Biomaterials*, 34 (2013) 5431-5438.
- [29]. M. Park, D. Lee, S. Shin, J. Hyun, Effect of negatively charged cellulose nanofibers on the dispersion of hydroxyapatite nanoparticles for scaffolds in bone tissue engineering. *Colloids Surf. B: Biointerface*, 130 (2015) 222-228.
- [30]. H. Morgan, R.M. Wilson, J.C. Elliott, S.E.P. Dowker, P. Anderson, Preparation and characterization of monoclinic hydroxyapatite and its precipitated carbonate apatite intermediate, *Biomaterials*, 21 (2000) 617-627.
- [31]. S. Brunauer, P.H. Emmett and E. Teller, Adsorption of gases in multi molecular layers", *Journal of the American Chemical Society*, 60(2) (1938) 309-319.
- [32]. E.P. Barrett, L.G. Joyner and P.P. Halenda, the determination of pore volume and area distributions in porous substances. I. Computations from nitrogen isotherms", *Journal of the American Chemical Society*, 73(2) (1951) 373-380.
- [33]. M. Mabrouk, Y.E. Choonara, T. Marimuthu, P. Kumar, L.C. du Toit, S. Vuuren, V. Pillay, Ca₃(PO₄)₂ precipitated layering of an in situ hybridized PVA/Ca₂O₄Si nanofibrous antibacterial wound dressing. *International Journal of Pharmaceutics*, 507 (2016) 41-49.
- [34]. T. Kokubo, *Bioceramics and their clinical applications*", Woodhead publishing limited and CRC Press LLC, Cambridge England, (2008) pp. 174-760.
- [35]. T. Xiu, Q. Liu, J. Wang, Comparisons between surfactant-template mesoporous and conventional sol-gel-derived CaO-B₂O₃-SiO₂ glasses: Compositional, textural and in vitro bioactive properties, *Journal of Solid State Chemistry*, 181 (2008) 863-870.
- [36]. K.S. Manupriya, K. Thind, V. Singh, G. Kumar, D.P. Sharma, et al., Compositional dependence of in-vitro bioactivity in sodium calcium borate glasses, *J. Phys. Chem. Solids* 70 (2009) 1137-11.

- [37].K.M. Tohamy, I.E. Soliman, A.E. Motawea, M.A. Aboelnasr, Synthesis, Characterization and Bioactive Study of Borosilicate Sol-Gel Glass. *Nature and Science* 13(8) (2015) 147-150.
- [38].U. Rottenstone, B. Sarker, D. Heusinger, et al, *In vitro* and *in vivo* Biocompatibility of Alginate Dialdehyde/Gelatin Hydrogels with and without Nan scaled Bioactive Glass for Bone Tissue Engineering Applications. *Materials*, 7 (2014) 1957-1974.
- [39].J.D. Bancroft, A. Stevens, D.R. Turner, *Theory and Practice of Histological Techniques* (forth ed.), Churchill Livingstone, New York (1996).
- [40].E. Beutler, O. Duron, B.M. Kelly, Improved method for the determination of blood glutathione. *J Lab Clin Med.*, 61(1963) 882–890.
- [41]. M. Mihara, M. Uchiyama, Determination of malonaldehyde precursor in tissues by thiobarbituric acid test. *AnalBiochem.* 86(1) (1978) 271-280.
- [42].S. Srinivasan, R. Jayasree, K.P. Chennazhi, S.V. Nair, R. Jayakumar, Biocompatible alginate/nano bioactive glass ceramic composite scaffolds for periodontal tissue regeneration, *Carbohydrate Polymers*, 87 (2012) 274– 283.
- [43].P.P. Lopes, F. Leite& M. Gomes, et al., Silicate and borate glasses as composite fillers: a bioactivity and biocompatibility study, *J. Mater. Sci: Mater.Med.* 22 (2011) 1501–1510.
- [44].A.M. Deliormanli, In vitro assessment of degradation and bioactivity of robocast bioactive glass scaffolds in simulated body fluid, *Ceram. Int.* 38 (2012) 6435–6444.
- [45].V. D. Sergey, Amorphous calcium (ortho) phosphates" *ActaBiomaterialia* 6 (2010) 4457–4475.
- [46].G. Bipin & C. Ambalangodage, Fabrication and characterization of carboxymethyl cellulose novel microparticles for bone tissue engineering, *Materials Science and Engineering C*, 69 (2016) 733–743.
- [47].Y.X. Luo, A. Lode, C.T. Wu, J. Chang & M. Gelinsky, Alginate/ Nanohydroxyapatite Scaffolds with Designed Core/Shell Structures Fabricated by 3D Plotting and in Situ Mineralization for Bone Tissue Engineering, *ACS Appl. Mater. Interfaces*, 7 (2015) 6541-6549.

- [48].Y. Han, Q.Y. Zeng, H.Y. Li, J. Chang, The calcium silicate/alginate composite: preparation and evaluation of its behavior as bioactive injectable hydrogels, *Acta Biomater.* 9 (2013) 9107-17.
- [49].J. Wang, M. Wang, M. Zheng, Q.Guo, Y. Wang, H. Wang, X. Xi, F. Huang, R. Gong, Folate mediated self-assembled phytosterol-alginate nanoparticles for targeted intracellular anticancer drug delivery. *Colloids Surf. B: Biointerface*, 129 (2015)63-70.
- [50].W. Lan, L. Yubao, Z. Yi, Z. Li, M. Yuanhua, H. Jimei, Study on the biomimetic properties of bone substitute material: nano-hydroxyapatite/polyamide 66 composite. *Mater Sci Forum*, 510-511 (2006) :938–41.
- [51].X. Zhang, Y. Li, G. Lv, Y. Zuo, Y. Mu, Thermal and crystallization studies of nano-hydroxyapatite reinforced polyamide66 biocomposites, *Polym Degrad Stabil.* 91 (2006) 1202–1207.
- [52].A. Wan, E. Khor, G. Hastings, Preparation of a chitin/apatite composite by in situ precipitation onto porous chitin scaffolds, *J Biomed Mater Res.* 41 (1998) 541–8.
- [53].M. Wang, S. Deb, W. Bonfield, Chemically coupled Hydroxyapatite-polyethylene composites: processing and characterization. *Mater Lett*; 44(11) (2000) 119–124.
- [54].M.M. Dicu, M. Abrudeanu, S. Moga, D. Negrea, V. Andrei, C. Ducu, Preparation of ceramic coatings on titanium formed by micro-arc oxidation method for biomedical application *Adv. Mater.*, 14 (2012) 125-130.
- [55].W. Xuejiang, L. Yubao, W. Jie, K. de Groot, Development of biomimetic nano-hydroxyapatite/poly(hexamethyleneadipamide) composites. *Biomaterials* 23(24) (2002) 4787–4791.
- [56].J. Wei, Y. Li, Tissue engineering scaffold material of nano-apatite crystals and polyamide composite. *Eur Polym J*, 40(3) (2004) 509–515.
- [57].Y. Zuo, Y. Li, J. Wei, J. Han, F. Xu, The preparation and characterization of n-HA/PA series biomedical composite. *Funct Mater* 35(4) (2004) 513–516.

- [58].Z. Xiang, L. Yubao, L. Guoyu, Z. Yi, M. Yuanhua, W. Lan, The study on interaction mechanism between n-HA and PA66 in n-HA/PA66 biocomposites. *Funct Mater*, 36(6) (2005) 896–909.
- [59].M. Wang, S. Deb, W. Bonfield, Chemically coupled Hydroxyapatite–polyethylene composites: processing and characterization. *Mater Lett*, 44(11) (2000) 119–124.
- [60].A . Borzacchiello, A. Gloria, L. Mayol, S. Dickinson, S. Miot, I. Martin and L. Ambrosio, Natural/synthetic porous scaffold designs and properties for fibro-cartilaginous tissue engineering, *Journal of Bioactive and Compatible Polymers*, 26(5) (2011) 437–451.
- [61].T. Patrício, M. Domingos, A. Gloria, U. D'Amora, J.F. Coelho, P.J. Bártolo, Fabrication and characterisation of PCL and PCL/PLA scaffolds for tissue engineering”. *Rapid Prototyping Journal*, 20 (2014) 145-156.
- [62].A.C.A. Wan, E. Khor, G.W. Hastings, Preparation of a chitin/apatite composite by in situ precipitation onto porous chitin scaffolds. *J Biomed Mater Res*, 41 (1998) 541–548.
- [63].R. Ulrike, S. Bapi, D. Heusinger, et al, *In vitro* and *in vivo* Biocompatibility of Alginate Dialdehyde/Gelatin Hydrogels with and without Nanoscaled Bioactive Glass for Bone Tissue Engineering Applications. *Materials*, 7 (2014) 1957-1974.
- [64]. B. Duan, L.A. Hockaday, K.H. Kang, J.T. Butcher, 3D bioprinting of heterogeneous aortic valve conduits with alginate/gelatin hydrogels. *J. Biomed. Mater. Res. Part A*, 101 (2013) 1255–1264.
- [65].F. Valenzuela, C. Covarrubias, C. Martinez, et al., Preparation and bioactive properties of novel bone-repair bionanocomposites based on hydroxyapatite and bioactive glass nanoparticles. *J. Biomed.*,100 (2012) 1672–1682.
- [66].E. Kozer, S. Evans, J. Barr, R. Greenberg, et al., Glutathione, glutathione-dependent enzymes and antioxidant status in erythrocytes from children treated with high-dose paracetamol. *ClinPharmacol*, 55 (2002) 234–240.

Figure legends

Fig. 1. TGA thermo-grams of prepared scaffolds sample

Fig. 2. Mechanical properties of prepared scaffolds sample, a) DE and b) RG.

Fig 3. Bar-graphs represents a) total pore volume b) BET surface area and c) pore diameters of the prepared scaffolds.

Fig.4. XRD patterns of scaffolds sample: a) before soaking in SBF; b) after soaking in SBF

Fig 5: FTIR spectra of scaffolds sample: a) before soaking in SBF; b) after soaking in SBF

Fig 6. (Top) SEM images of the scaffolds samples S and SH40 before (a, b) and after (c, d) soaking in SBF. (Bottom) The same SEM (e1 and f1), (e3 and f3) images after treatment with the flooding algorithm in SXWM software and EDX (e3 and f3). The blue areas represent the calcium phosphate-free surfaces.

Fig. 7 Photomicrograph of histopathological examination of femur bone defects after 6 weeks implantation; a) control rats holes without any matrix filler; from b: f image holes with S, SH, SH10, SH20 and SH40 scaffolds filler respectively. Osteocytes at the periphery of the fractured ends (OC) with inflammatory cells infiltration (IF) and filling of the fracture gap with granulation tissue (GT) and newly formed bone (NB).

Fig. 8. Liver histopathological examination after 6 weeks of implanting the matrix; a) Control rats, b): Matrix-filled bone rats with S scaffolds, C):SH, d):SH10, e): SH20, f): SH40 filler scaffolds respectively.

Fig. 9. Histograms of blood biochemical examination for rats after 6 weeks of scaffolds implantation; a) sGOT, b) sGPT, c) sGSH and d) sMDA. All data are represented as mean \pm SEM. One way ANOVA statistical test was used to compare significance with Tukey's post-Hoc test.

Table 1: Different composite scaffolds

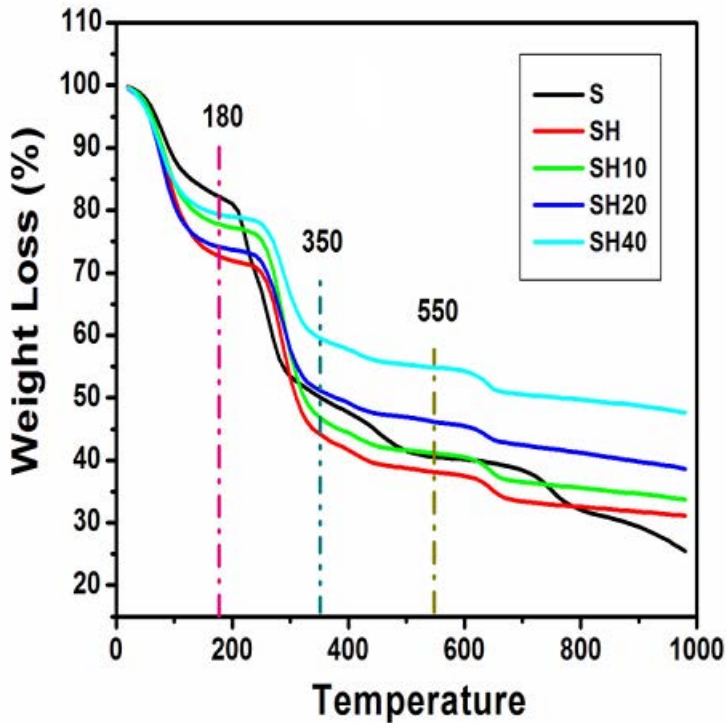
Sample code	S	HEC	HA
S	100	0	0
SH	50	50	0
SH10	50	50	10
SH20	50	50	20
SH40	50	50	40

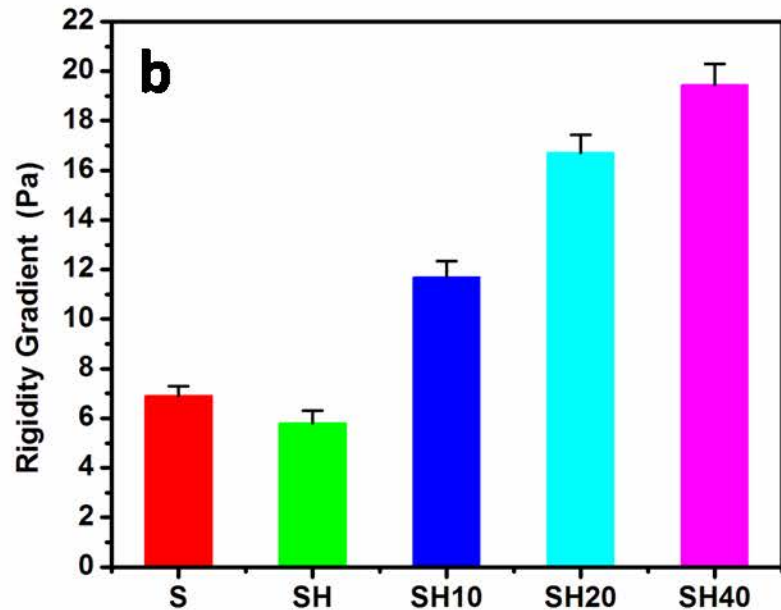
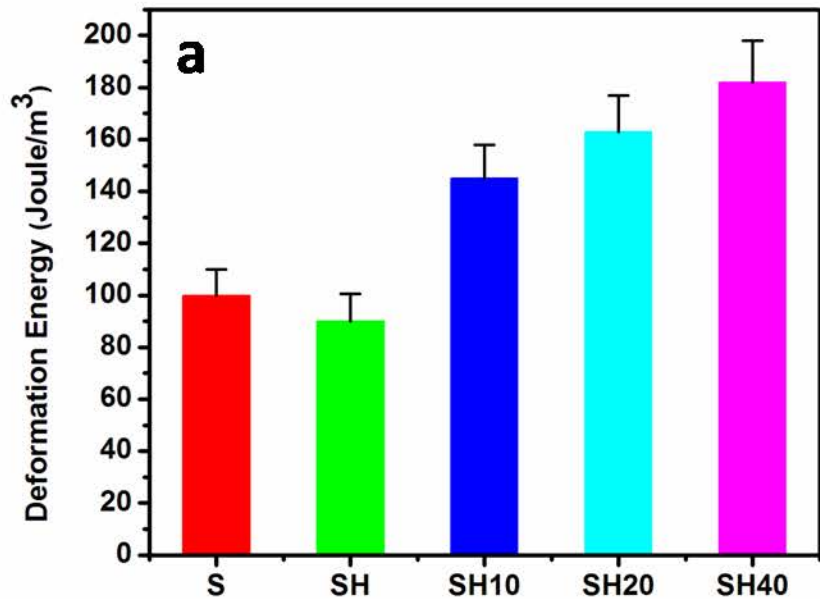
Table 2: Weight loss for all prepared samples at different temperature.

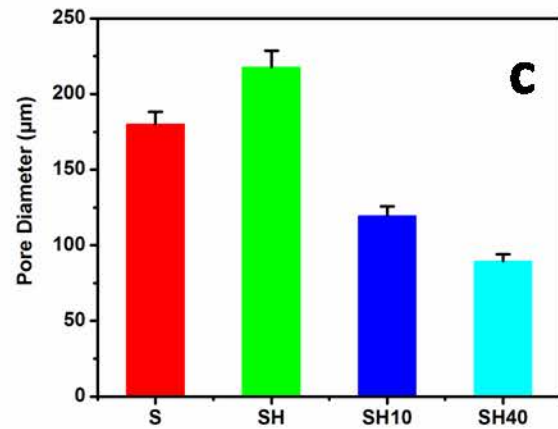
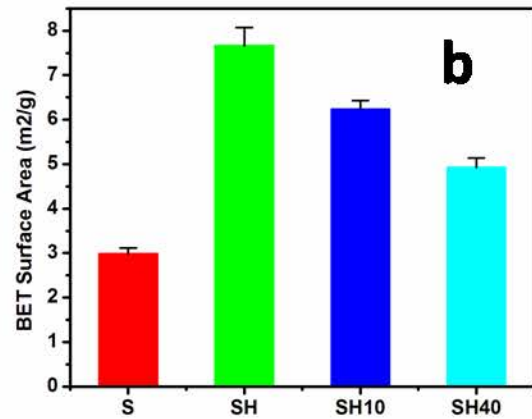
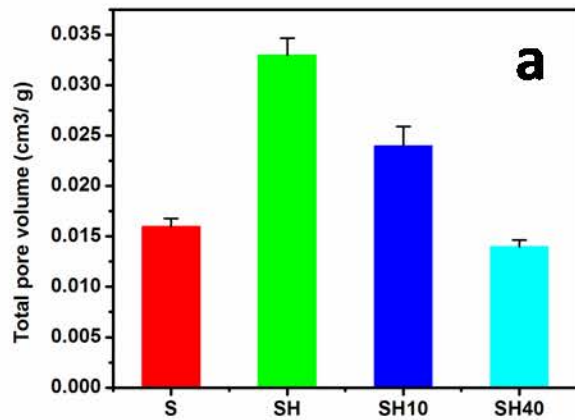
Samples	100°C	180°C	340°C	1000°C
S	11.6	17.8	49	70.5
SH	17.5	27.3	55	68
SH10	15	21.8	52	65
SH20	18.6	25.5	48	59.8
SH40	14.4	19.66	38	50.7

Table 3: BET surface area and porosity factor measurements of the prepared scaffolds

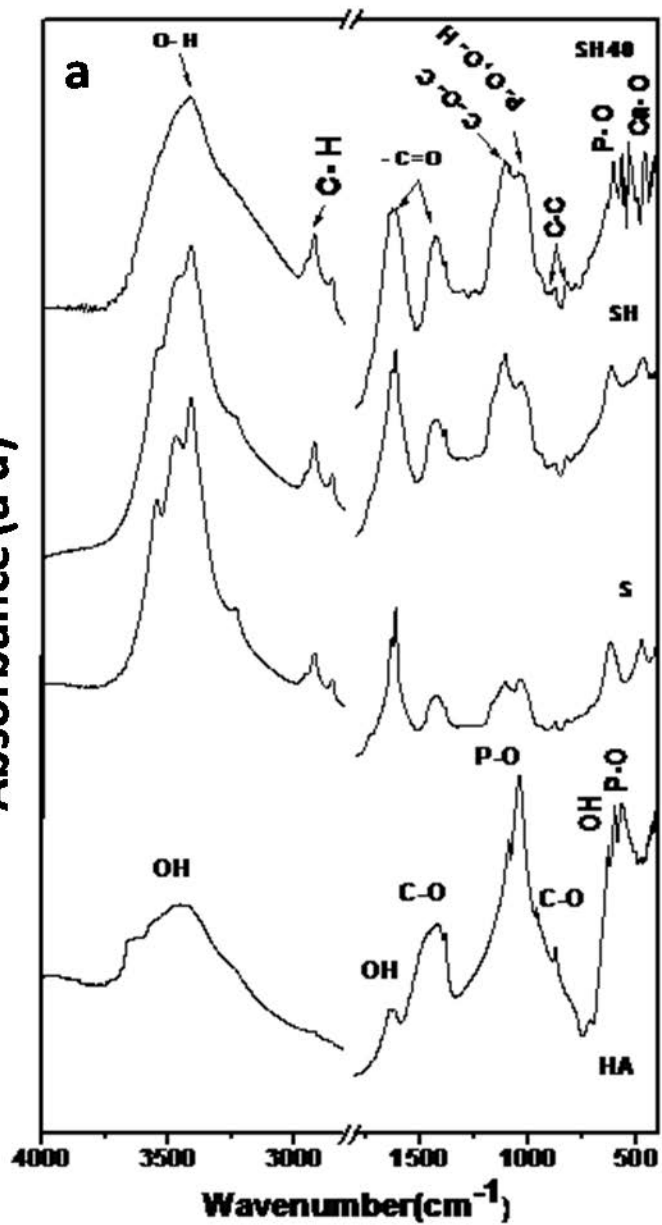
Sample	BET Surface Area (m²/g)	Total pore volume (cm³/ g)	Pore Diameter (μm)
S	2.983± 0.129	1.5793 × 10 ⁻²	179.96±8.42
SH	7.6593±0.4124	3.286 × 10 ⁻²	217.7±10.87
SH10	6.2314±0.1982	2.38675× 10 ⁻²	119.5±6.29
SH40	4.9213±0.2156	1.3529× 10 ⁻²	89.5±4.58



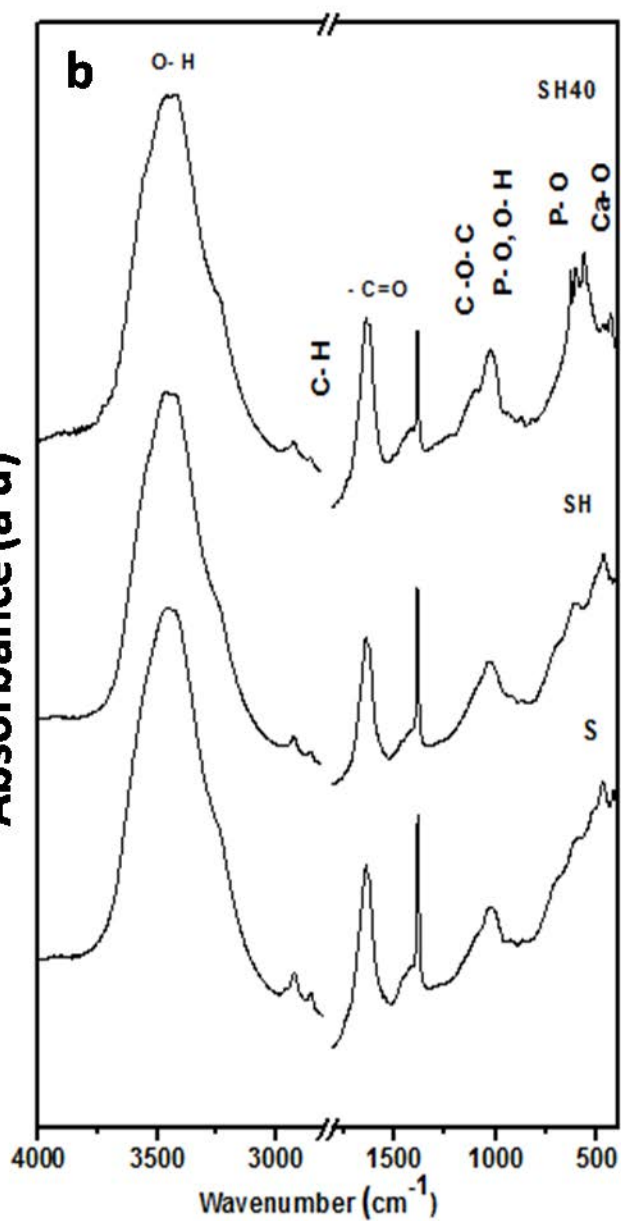


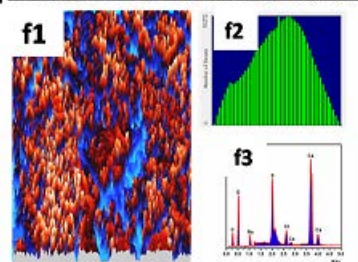
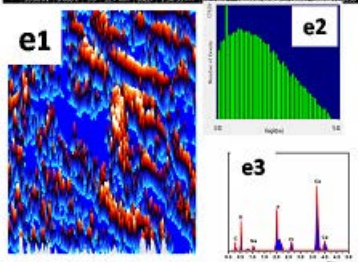
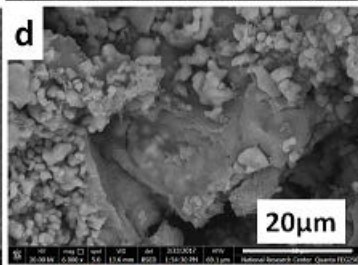
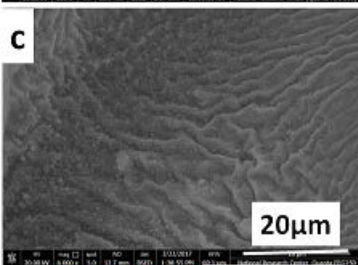
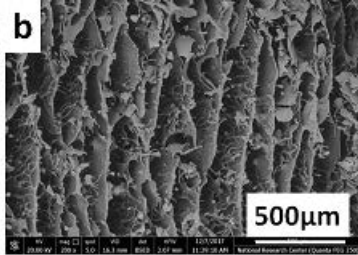
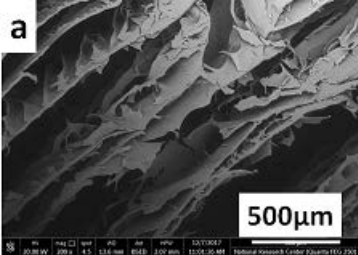


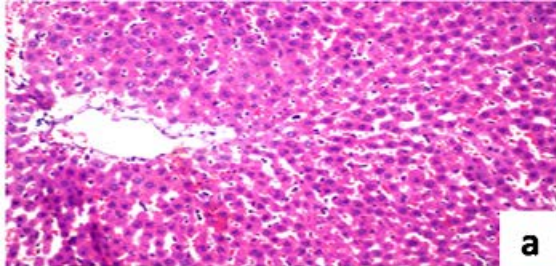
Absorbance (a u)



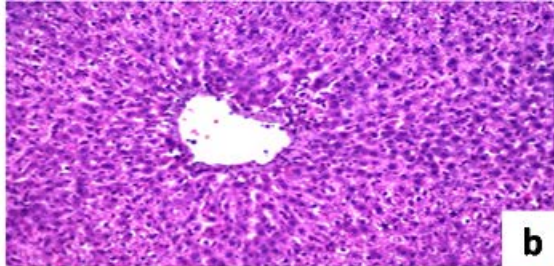
Absorbance (a u)



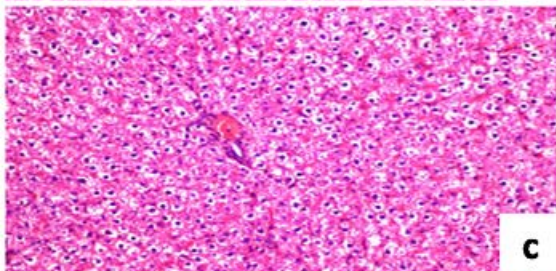




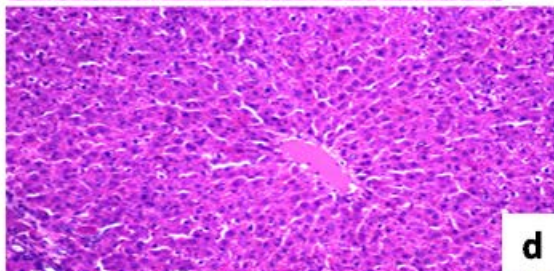
a



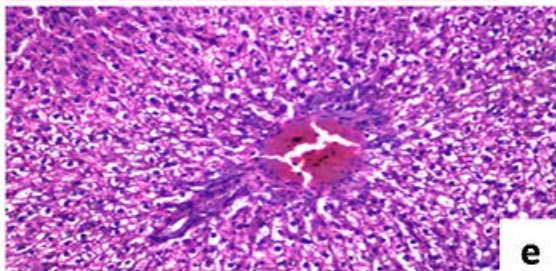
b



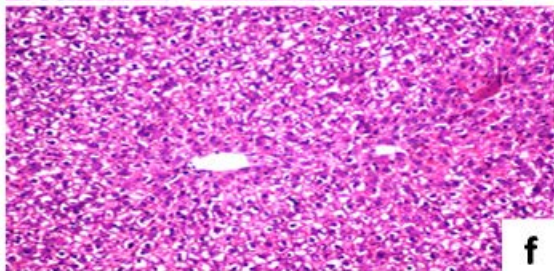
c



d



e



f

